

SYNTHESIS REPORT

FOR PUBLICATION

CONTRACT N° : **BREU CT91 0563**

PROJECT No : **BE 4398**

TITLE :
**Non Contacting Surface Characterisation of Ceramics and
Coatings with Micro Acoustic Waves**

C - MAW

PROJECT
COORDINATOR : **Rolls-Royce plc**

PARTNERS :

**SKF ERC BV (NL)
NMRC Cork (Irl)
IWT Breman (D)
Nottingham University (UK)**

Sponsors:

**T & N (UK)
Peugeot (Fr)**

1st June 1992 to 31st May 1995

STARTING DATE: 1st June 1992

DURATION : 36 MONTHS



**PROJECT FUNDED BY THE EUROPEAN
COMMUNITY UNDER THE BRITE/EURAM
PROGRAMME**

DATE : 6th Feb 1996

2. Title

Non-Contacting Surface Characterisation of Ceramics and Coatings with Micro Acoustic Waves

Authors: A. K. **Dunhill** (RR) T. **Flaherty** (NMRC)
R. **Cundill** (SKF) M. G. **Somekh** (N. U.)

3. Abstract

The goal of this project is to demonstrate novel laser generated ultrasonic inspection techniques to measure accurately the velocity of surface acoustic waves (V_{SAW}) in engineering **ceramics** and coatings. All acoustic wave velocities are affected by the state of stress in the material they propagate. High **frequency** SAWS are confined to near to **surface** regions and are **affected** by surface stresses and defects which, in these materials tend to lie within the first **10 μ m**. The project demonstrated the change in V_{SAW} with stress in typical industrial materials and **components** and showed that this method could provide a nondestructive means of process optimisation and control.

4. Introduction

Ceramic materials and coatings in the **electronics and** especially industrial sectors have had limited use due to poor performance often caused by the manufacturing processes. These processes, machining, coating heat treatment etc. impart regions of high residual stress and damage in the **surface layers**. These in turn reduce the performance of the components, By optimizing the processing parameters the stresses and damage can be **reduced**, improving the reliability. At present optimisation is established through extensive 'trial and error' testing. This is expensive and inefficient and does not provide a means of process control.

The partners, in this project recognised that **accurate Surface** Acoustic Wave (SAW) velocity measurement techniques could address this limiting aspect of engineering ceramics and that the existing methods required great care to achieve the necessary accuracy.

Initially only one system was envisaged **but**, the range of **surface** roughness presented by the partners dictated that two systems were **needed**, one tailored for smooth surfaces, as required by the engineering partners and one for the electronics components which are rougher as they are used as multi-layer packaging materials.

For the engineering applications the continuous wave **system**, operating at a frequency of **82MHz** at Nottingham University, has been developed. The predicted measurement accuracy's of 1 in 2000 have been achieved and changes in V_{SAW} of **15m/s** have been measured when high stresses have been applied to the ceramic materials.

For the **electronic** packaging materials, which constituted the rough surface samples, there was a slightly different requirement in so much as an **incoming** inspection was required to ensure the consistency of the supplied material. To inspect as much material as possible a low frequency was used so that the wave **would** occupy as much of the **1mm** thick **wafers** as possible.

The programme succeeded in achieving the objectives and deliverables within budget,

5. Technical Description

The following steps were taken to **develop** the measurement **system**:-

- Manufacture ceramic samples in materials chosen by the industrial users with low states of **surface** stress and ideal **geometry**, i.e. flat bars, and carry out sample validation exercise to ensure the physical and optical properties of the chosen materials was well understood.
- **Design**, build, and test a stressing jig to take the ideal samples and calibrate the strain (and hence stress) induced in the bar for a given load in the jig, using X-ray diffraction.
- Design, build, and test non contacting laser based SAW generation **and** detection systems. Both a continuous wave and pulsed C-MAW system were produced to cover the range of **surface** finishes required by the industrial partners.
- Use stressing jig in conjunction with the C-MAW system and measure the **surface** acoustic wave velocity (V_{SAW}) at different stress levels and determine the magnitude of the change of V_{SAW} with stress in the chosen materials.
- Determine the applicability of this measurement method to the materials and components of interest to the industrial partners.

5.1 Samples .-”

Ideal samples were defined in terms of materials, form and **geometry** and surface condition principally to provide reference samples for the development of the C-MAW technique and for measurement and calibration of surface stresses. In **addition**, other ideal samples were specified for material characterisation and validation, determination of optical characteristics, acoustic wave velocity measurements and other purposes, Industrial samples were also **defined** to cover a range of materials and components **produced**, or under development by the partners and sponsors.

All the ideal **samples** used for the C-MAW system were specified to be supplied in the **fine** ground or lapped condition having a **surface** roughness of less than 0.1 $\mu\text{m Ra}$. However silicon nitride samples with higher **surface** roughness up to 0.6 $\mu\text{m Ra}$ were also included to investigate whether the technique could be applied to ground components. Highly polished **surfaces** were required for the determination of **optical** characteristics and evaluation of material response to exposure to high intensity laser beams.

The hydraulic stressing rig designed and produced by **IWT** required large specimens to allow access for X-ray beams under 4-point loading. These specimens were of the form of rectangular bars (150x 10 x 3 or 5 thick). Different thicknesses were specified to give different **sub-surface** stress gradients.

Since not **all** materials of **interest**, particularly ceramic materials, could be **fabricated** into such large specimens, a smaller stressing rig was also constructed to accommodate bars of 50 x 3x 3 or 5mm. This type of specimen was similar to standard modulus of rupture test pieces used for determination of the strength of ceramic materials.

5.1.2. Sample validation

The following evaluation methods were used.

Metallographic analysis

Ceramic Samples

Macro & Micro
X-ray phase analyses
Hardness, toughness, density & surface finish.

Steels Samples

Micro
Hardness
Chemical composition

All Samples

SEM (NMRC & T&N)

Penetrant testing (SKF)

50MHz UST (whole bar) (RR)

200MHz UST (5mm² stressed area)
(IWT)

High definition radiography (RR)

V_{LONG} and V_{SHEAR} measurements
(NMRC & RR)

Optical properties (NMRC)

Mechanical testing, Rolling contact fatigue (SKF)
& Modulus of rupture (T&N)

Some of the tests were inappropriate for the samples and so only the relevant ones were carried out. The test method of some of these is given below.

5.1.3. Penetrant inspection

This was undertaken by SKF where the penetrant testing facilities have been developed especially for ceramic materials and a high sensitivity for surface breaking flaws has been achieved using a new standard fluorescent dye technique with microscope viewing. No defects other than minor edge chipping, well away from the middle of the specimens, were observed.

5.1.4. 50 MHz ultrasonic inspection

This inspection is based on pulse/echo detection of internal reflectors using a focused 50 MHz transducer. The focal length was 25 mm in water. This gives an inspection depth range of 2→5 mm in SiN and SiC and each bar was inspected from the top (chamfered) and bottom (flat) faces. The scan system produces a x16 printout of each sample. To ensure the same sensitivity was achieved barSS101 was used as a control piece. The number of indications found on each bar was recorded and their position can be found by reference to the original scans, kept within the NDE Group at RR, Bristol,

5.1.5. 200 MHz ultrasonic inspection

This inspection was carried out to give an indication of the material imperfections in the near surface region where the C-MAW measurements will be taken.

The acoustic microscope of the IWT was used in the reflective mode with ultrasonic frequencies of 100, 200 and 400 MHz. The acoustic images were obtained by horizontal lens scanning. On the samples with low surface roughness pores were detected.

No significant **features** were seen indicating these **samples** were of high enough **quality** for the programme.

5.1.6. High definition radiography

The inspection uses the X-Tek **microfocus** x-ray, real time, system with a spot size of **5 μ m** and is sensitive to >1% changes in component density. Magnification of up to x20 was used.

Each bar was scanned in two directions **perpendicular** to the **axis** of the bar and the position of each indication noted. The size of the indications was established using a 320 μ m wire strapped to the sample. The results and X-ray images have been kept at the RR **NDE** group Bristol. The **largest** indications were seen in Bar SS 102 at 120 μ m.

5.1.7. V_{LONG} and V_{SHEAR} measurements

An **Olympus UH3 scanning acoustic** microscope, with 50 MHz lens of 14° half aperture was used for mechanical property determination and imaging. The longitudinal and shear wave velocities have been measured and the SAW velocities for the materials calculated. Young's modulus and Poisson's ratio have also been calculated for each **sample** from this data.

These values were found to be high for the materials and a repeat measurement was made using a different **method** developed at RR. This technique requires a shaped **aluminium** wedge to be glued to the sample and **an** incident ultrasonic beam is **refracted** at the wedge to produce either a normal incident, shear or longitudinal wave onto the sample,

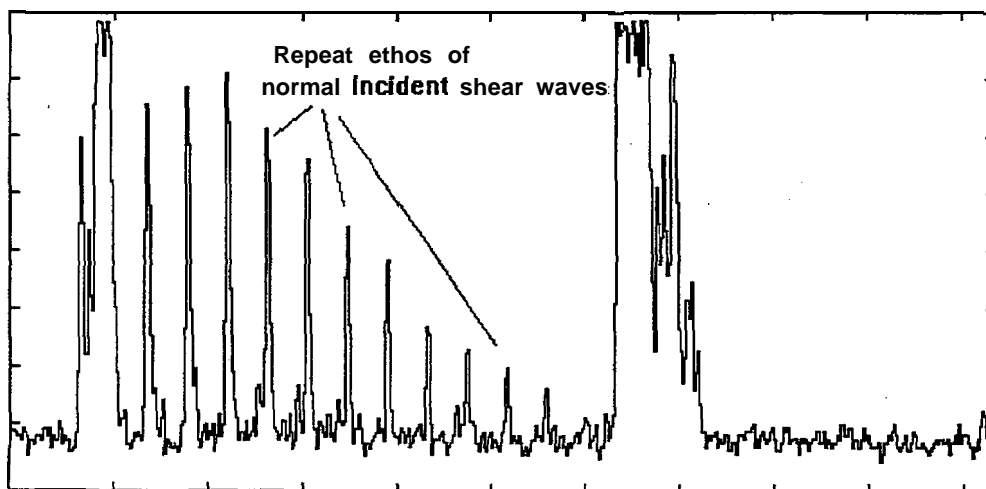


Fig 1 Typical signals for shear velocity measurement

5.1.8. Optical characterisation

The optical characterisation samples were polished on one side to optical smoothness. The samples ranged in **colour** from white (**Al₂O₃**) through a mixture of **greys** and **yellows** (**ZrO₂**) to black (**Si₃N₄**). Variations in **colour** across some of the samples indicated poor mixing of the constituent phases. Spectroscopic **ellipsometry** studies have been carried out on the samples to determine their optical properties. The SE studies permit the measurement of the refractive **index**, **n** and the dielectric **constant**, **k** of the samples as a **function** of wavelength and hence, the **reflectivity** and the absorption coefficient at

specific wavelengths i.e. pulse and probe laser wavelengths. The SE spectra have shown interesting variations according to sample phase, preparation and composition. Each spectrum **also** contains the information necessary to calculate the reflectivity and absorption coefficient. for the sample at the probe and pump **wavelengths** of 633 and 532nm. The recorded spectra are presented in the appendix and indicate some interesting results, especially in relation to the silicon carbide whisker reinforcement of silicon nitride, Sample CDL is Si_3N_4 , sample CMC is Si_3N_4 with SiC whiskers and sample CVD is SiC . An increase in the value of n with increasing SiC content is apparent. Fourier transform infra-red spectroscopy analysis was applied to these ceramic samples to investigate the **infra-red** reflectance spectrum in the wavelength range 2-25 μm . Spectra for α and β phase SiN presented in Fig 2,

The difference between the spectra of α and β -silicon nitrides is **marked**, especially in the 10 and 17 μm regions and shows the FTIR technique to have considerable potential as a non-destructive technique for ceramic phase **analysis**.

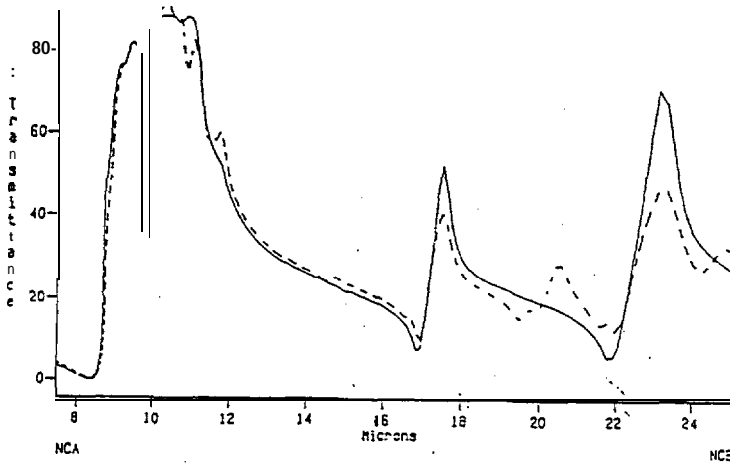


Fig 2 FT-IR spectra for α -(broken line) and β -(unbroken line) phase silicon nitride ceramics

5.2.1. Design and manufacture of stress generation jigs

Two 4 point bending jigs using a hydraulic force for the loading and a large bar sample (150x 10x 5) were built. The hydraulic load was controlled by a PC, which enabled an automatic check of the bending **load** during use. Two smaller hand operated jigs were also built to enable the *smaller* samples to be evaluated.

The strain generated in the samples was measured using X-ray **diffraction** and calibration curves produced for the **ideal** samples.

5.2.2 X-ray diffraction

The X-ray diffraction **examinations** for the steel samples have been executed by a computer controlled ψ -**diffractometer** with vanadium **filtered Cr-K α -radiation**. The interference line of the α -iron {211}-lattice **plane** was measured with a step size of $0,1^\circ$ in 2Θ for an interval of $2\Theta = 10^\circ$ and a measuring time of 3 sec per step. Lattice strains were determined for ψ angles = $0^\circ, \pm 7^\circ, \pm 20^\circ, \pm 30^\circ, \pm 40^\circ, \pm 45^\circ$ after a linear lattice strain distribution against $\sin^2\psi$ was proved. The $\sin^2\psi$ method with macroscopic elastic constants were used for the residual stress determination. The penetration depth of **Cr-K α -radiation** into steel is about 5 μm for $\sin^2\psi = 0.3$.

For the ceramic specimens a suitable interference **line** for residual stress measurements was chosen after a phase analysis. The interference line of the Si_3N_4 {411} and {510} -lattice planes were measured with a step size of 0,050 in $2\Theta = 2^\circ$ and a measuring time of 10 seconds per step. Residual stresses are

calculated from lattice strains at ψ -angles discussed above using X-ray elastic constants of $\frac{1}{2}S_2 = 4 \times 10^{-6} \text{ mm}^2/\text{N}$. A typical calibration line is shown below:-

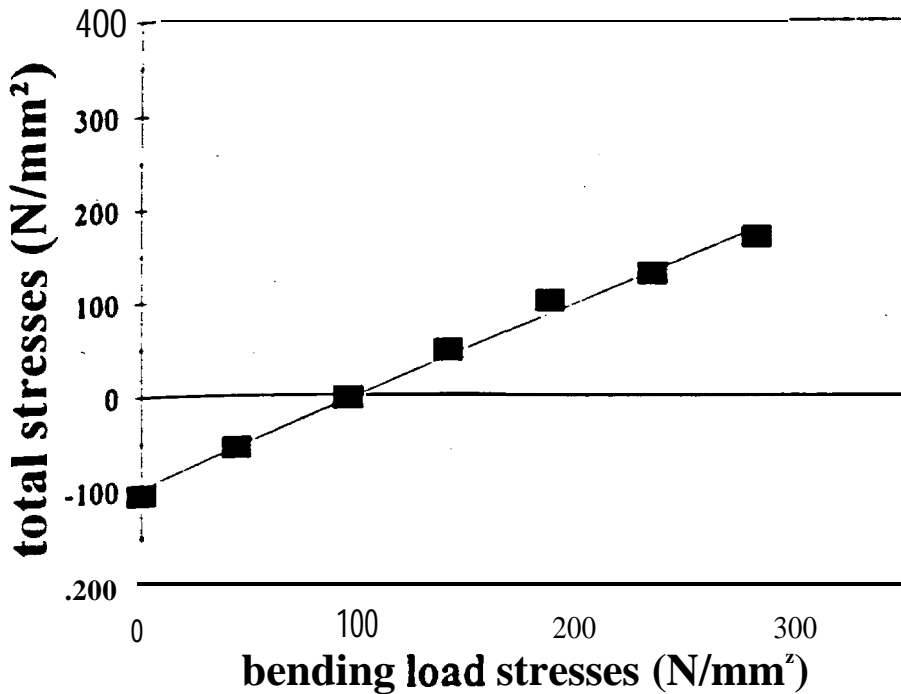


Fig. 3 Sample SS1 11, X-ray measurements of total stresses v bending stresses

5.3.. Laser SAW system

5.3.1. Detection

As the generation and detection systems were being developed in parallel SAW devices were used to evaluate the detection designs in the early stages of the programme. A number of interferometer designs were investigated including direct and indirect heterodyne systems. The system chosen for both the pulsed and CW instruments was the stabilised homodyne interferometer which requires no extra signal processing and the wideband signal from the SAW pulses can be recorded directly from the interferometer output,

To avoid the complexity of the heterodyne interferometers, a homodyne interferometer has been constructed, as shown in Fig 4. After passing through an optical isolator the light passes through the beamsplitter onto a Wollaston prism where the two orthogonal polarisations are split in angle so that they focus on adjacent points on the sample. These two beams are then reflected back through the system, with their polarisation so adjusted that beam A interferes with RA and B interferes with RB, whose outputs are detected at DA and DB respectively. The system thus operates as two interferometers in parallel. The output signal from detectors DA and detectors DB contain a fixed level output resulting from the maintenance of the interferometers at the position of best sensitivity with a small perturbation superimposed which arises when the surface acoustic wave passes under the corresponding probe beam. This homodyne configuration is particularly suitable for pulsed surface waves since no extra hardware signal processing is required for wideband signal from the pulses maybe recorded directly from the interferometer output. The two probe beams provide differential measurements of the delay time which can greatly eliminate the timing jitter due to amplitude fluctuations and to give very high accuracy of measurement in the velocity change, up to 1 part in 10^4 .

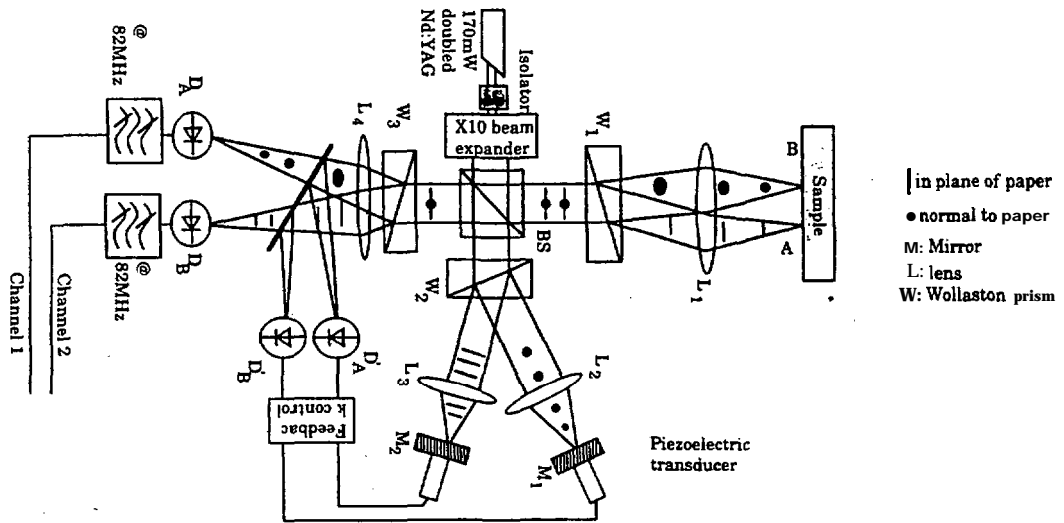


Fig 4 Detection configurations of the dual beam SAW measurement system

Since the **interferometers** are **homodyne** the sensitivity to displacement varies sinusoidally, it is thus necessary to maintain each beam operating at a sensitive point. To do this, a **feedback** control has been implemented in order to lock the **sensitivity** of the interferometer to its highest level. A portion of the output signal from the each arm is detected by **detectors** D_A and detectors D_B respectively. The low pass filtered output from each of these detectors is then fed into a comparator, which compares the output with a reference value so that deviations from the desired level are fed back to the respective piezo pusher, thus correcting the phase of the **reference** beam so that a fixed operating point for the system is maintained. The extraction of the SAW velocity information is **performed** on a PC using MATLAB for the **CW** system,

5.3.2. Errors in SAW measurement

The principal limitation in the measurement of absolute **velocity** is the accurate determination of the probe separation. This has been measured by scanning a knife edge across the two probes and determining the separation from the transition, this gives an uncertainty of approximately 1 part in 1000, This is acceptable since we are **concerned primarily** with measuring changes in SAW velocity. If, however, we wished to **further** enhance the absolute accuracy a fringe counting interferometer **can** be attached to the scan stage.

For our applications relative changes in velocity are of **far** more importance than absolute velocity measurement. The factors that lead to uncertainties in the relative velocity measurement relate the possible errors in the timing between the two probes. One instrumental source of such an error is the jitter inherent in the digital oscilloscope. This was tested by inputting two identical (noiseless) **82MHz** sinusoidal signals into each channel of the digital oscilloscope and measuring the apparent delay over a series of measurements, The **RMS** value of this uncertainty was found to be 3ps.

One **fundamental** source of error whose ultimate limit is set by the signal to noise of the SAW detection process is timing errors caused by variation in SAW amplitude. In order to relate the timing error to the input S/N ratio a series of computer simulations were performed. A tone burst with a Gaussian envelop was added to randomly generated noise so that the input S/N ratio could be varied. The resulting signals plus noise were then passed through the **processing** algorithm so that variation in the measured delay between the two signals could be calculated. The timing **uncertainty** as a **function** of input signal to noise ratio was calculated to be 8ps on a S/N ratio of 12.5 **dB**

Another possible source of error that was identified related to the variation in the output power of the laser between pulses. This means that setting the trigger to a fixed **level** translates to timing jitter of the

trigger point because the time that a **pulse** reaches a particular level is determined by the ultimate height of the pulse. **If** the time between excitation of the pulse and detection by a single pulse was used this would be a very severe source of error, In the two beam **configurations** we use here the effect is **largely** eliminated because the system measures the time delay between the probes so that the timing jitter due to amplitude fluctuations is common to each beam.

Another source of error relates to the variation in ambient temperature. Clearly temperature variation **affects** the actual sound velocity of the wave propagating through the **sample** (by typically **1m/s** per degree K), moreover the change in **temperature** will alter the separation of the probes, reliable measurements are thus clearly achieved when the temperature is stabilised. Table 1 gives measured velocities on a sample of silicon nitride as the ambient temperature is varied. The results indicate the excellent stability of the system when the temperature is stable.

If the temperature is stabilised and the jitter errors are **uncorrelated** we may expect **an RMS** timing error of $\approx 8.5\text{ps}$, for a beam separation of **1.1mm** this corresponds to an uncertainty in **relative** velocity for silicon nitride with a nominal SAW velocity of **5800m/s** of approximately **0.26m/s** or one part in 20,000.

Table 1 SAW velocity variation with temperature drift

Temperature (°C) during measurement	SAW velocity (ms ⁻¹)	Remarks
24.9 -25.4	5675.3	Heaters are used to
26.3 -26.4	5678.6	increase the room
27.9 -28.2	5672.3	temperature
28.9 -29.1	5668.3	
26.0 -26.3	5671.4	No heaters
25.7 -26.4	5671.6	
25.9 -26.3	5670.6	
25.7 -26.0	5671.6	

5.3.3. Sensitivity of interferometer to surface displacement

An experiment assessing and demonstrating the pulsed SAW detection displacement sensitivity was carried out by driving the piezo stack on which the **reference** mirror was mounted with a sinusoidal **voltage** **varying amplitude**. The amplitude of the piezo extension was calibrated and **carefully monitored**. The piezo extension coefficient is $0.15 \mu\text{m/V}$. The sensitivity of the interferometer to a calibrated displacement of between 10 and 400 nm was measured in the first calibration experiment. This experiment was repeated for the small-displacement *regime* **and shows the** interferometer to be sensitive to displacements of the order of 0.2 nm.

5.3.4. Generation

All possible methods for non-contact laser generation were reviewed and two systems were built.

5.3.5. Moving fringe generation

The modulation of a laser beam maybe achieved by interfering the **0th** and **1st** order beams **coming** out of a Bragg cell (**Fig.5**). The interference pattern **occurring** on the sample **surface** will appear as moving gratings. With the angle of incidence at the sample carefully chosen so that the **interference fringes** formed on the sample **surface** matched to the SAW wavelength of the sample, efficient generation of SAW on the sample should be achieved whilst spreading the heating to avoid damage of the sample,

The advantage of this method is that the frequency of SAW generated is dependant on the optical configuration and therefore variable

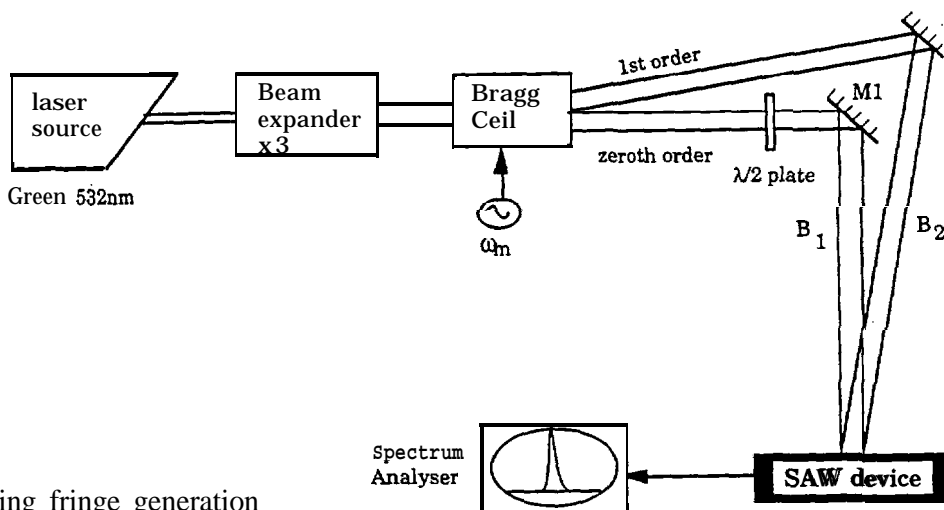


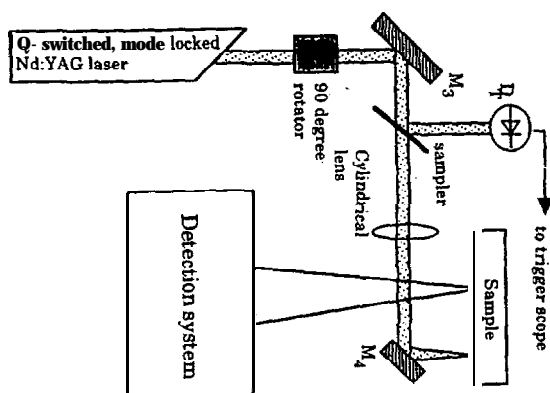
Fig 5 Moving fringe generation

To determine the effectiveness of this regime it was tried on a lithium niobate SAW device whose surface was painted black for maximum absorption. The light source used was a frequency-doubled Nd:YAG laser with a wavelength of 532 nm. The Bragg cell is driven by a signal at 103.5 MHz. At this driving frequency the angular separation between the 0th and the 1st order beams is approximately 5 degree. The rf power into the Bragg cell is adjusted such that the 0th and the 1st order beams are of equal optical power. The two beams are directed by two mirrors onto the SAW device to generate the required moving grating. The angular separation between the two incident beams has been estimated to be 0.802 degree in order to match the SAW wavelength of lithium niobate (38 pm). The gratings and the corresponding SAW generated by them will move unidirectionally on the sample. With the current setup SAW signal of signal-to-noise ratio up to 20B was observed.

5.3.6. Q switched mode locked generation

The Nd:YAG laser has been modified so that it can operate in Q-switched and mode-locked modes simultaneously. This means that the output of the laser consists of tone burst of high power pulses. The tone burst has a repetition rate adjustable between 10 Hz to 30 KHz. In our experiment a repetition rate of 1 KHz has been chosen because this gives the highest peak power. with each tone burst there are 33 narrow laser pulses which are approximately 400 ps wide and their repetition rate is 82 MHz. As shown in Fig 3.4.4.1 the Nd:YAG (pump) beam is focused into the sample surface to form a line 5 mm in length and 15 μm in width using a cylindrical lens. This leads to the generation of surface acoustic waves in the form of tone burst, The existence of such wave on a silicon nitride sample as been confirmed by observing the corresponding received electrical signal from a wedge transducer mounted on the sample surface.

Fig 6 Q-switched, mode-locked laser generation system



5.3.7. Optimum generation scheme

The principle of moving fringe generation of SAW waves has been demonstrated. This **single** frequency CW system can provide high accuracy of velocity measurement. However the small angles required for the two beams and the invisibility of the pump laser make the alignment of the system very **difficult**. In addition it requires a large average power compared to a pulsed system in order to generate measurable surface wave amplitudes, this will result in considerable background (DC) heating over the sample. On the other **hand**, in order to recover an accurate velocity measurement from a pulsed system it is **necessary** to extract the component in a very narrow band, this means that only a small fraction of the energy is used in the measurement. This problem **becomes** increasingly severe as the frequency is **increased**, since the **lower** ultrasonic frequencies are excited more efficiently than higher frequencies. The peak optical powers on the surface are therefore very **high**, so although the DC heating is **manageable**, **damage can** result from a high powered **single pulse**.

The Q-switch mode locked laser system which combines the advantages of both continuous wave and **pulsed** systems can provide the solutions to generate high peak power pulses without damaging and sample and maintain a high measurement accuracy. **It** was thus determined that the Q-switch mode locked laser system **should** be used.

As a means of **further** increasing the SAW wave amplitude zone plates were developed to produce a curved generation line to focus the SAW as it propagates along the **surface**.

5.3.8. Pulsed SAW generation system

For the pulsed C-MAW system the pump **laser** was a pulsed **Nd:YAG laser** operating at **fundamental** and 2nd harmonic wavelengths of 1064 and 532 **nm** respectively with a temporal pulse width of 7 **nsec**. The SAW pulse is generated by the **thermo-elastic effect** of the **laser pulse**. The laser beam is focused to a line shape on the sample surface using a cylindrical lens. This laser beam geometry was **selected** for two reasons: firstly, it enables a greater amount of laser energy to be coupled into the **sample** without reaching the ablation damage threshold of the material, and secondly, an acoustic **line** source leads to lower acoustic energy dissipation **in** the direction of propagation normal to the **line** where the detection probes will be. A small **fraction** of the laser beam is sampled and the pulse to pulse energy stability of the laser is thus monitored so that variations **in** SAW amplitude arising *from any* such instability **can** be compensated for. The setup is similar to the CW system in Fig. 6.

5.3.9. Prototype CW SAW Measurement system

The all-optical SAW generation and **detection** system is shown in Fig 7. In our experiment repetition rates of 1-5 KHz of tone bursts have been chosen because these give the highest peak power. Within each tone burst there are 33 narrow laser pulses which are approximately 400 ps wide and their **repetition** rate is 82 MHz. As shown in Fig 3.6.1,1 the **Nd:YAG** (pump) beam is focused into the sample **surface** to form a line 5 mm in **length** and 15 μ m in width using a cylindrical lens. For the **optical detection** of the surface waves, a dual probe system has been constructed with two **homodyne interferometers** in parallel. A **feedback** control has also been implemented in order to lock the sensitivity of the **interferometers** to their highest level, Atypical SAW signal detected is shown in Fig 8.

5.3.11. Prototype pulsed SAW Measurement system

Following the demonstration of the laser generation of surface acoustic waves on the SAW **devices**, and the measurement of the sensitivity curve of the SAW detection interferometer, the two systems were integrated into a single experimental set-up. The first part of this task was to design the **opto-mechanical configuration** of the integrated prototype. Key issues included the access of the pump beam to the **sample** under test, as well as working distance and positioning of focusing lenses. These issues

were resolved and a working prototype assembled. Evaluation of the complete system in the new configuration was then carried out. The first generation and detection of acoustic waves with the integrated optical system was on a silicon wafer. The recorded waveform is shown in Fig 9. The acoustic wave shows the classical Lamb wave shape due to the thickness of the wafer (0.5mm) and the centre frequency of the generated acoustic wave (≈ 1 MHz).

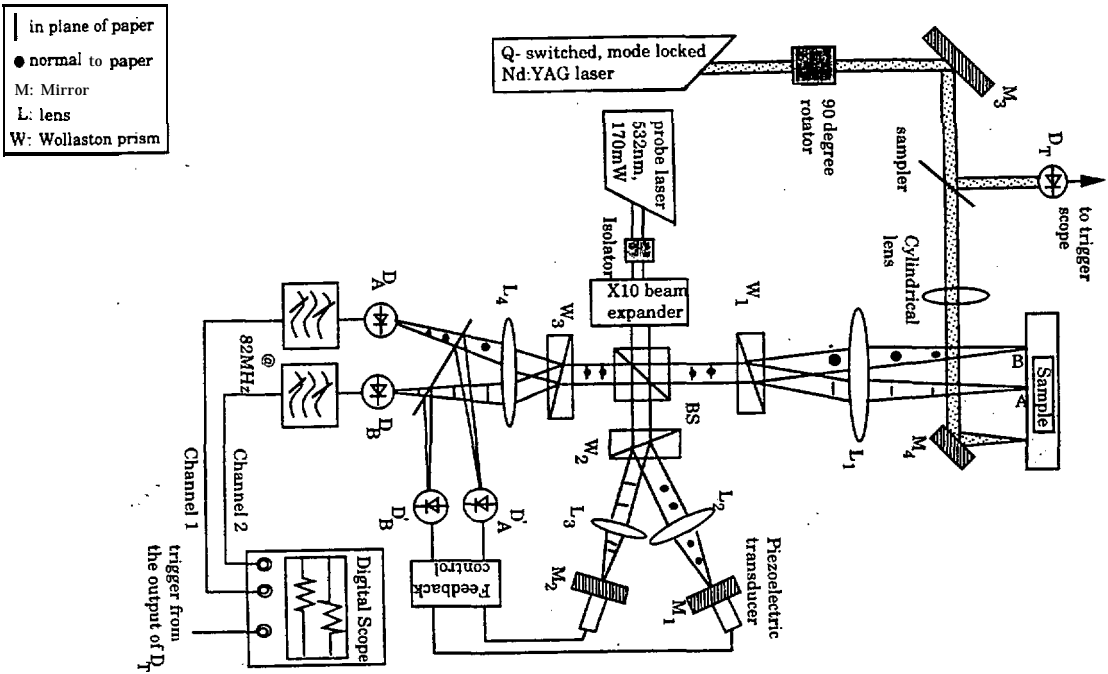


Fig 7 Diagram of the complete CW surface wave measurement system

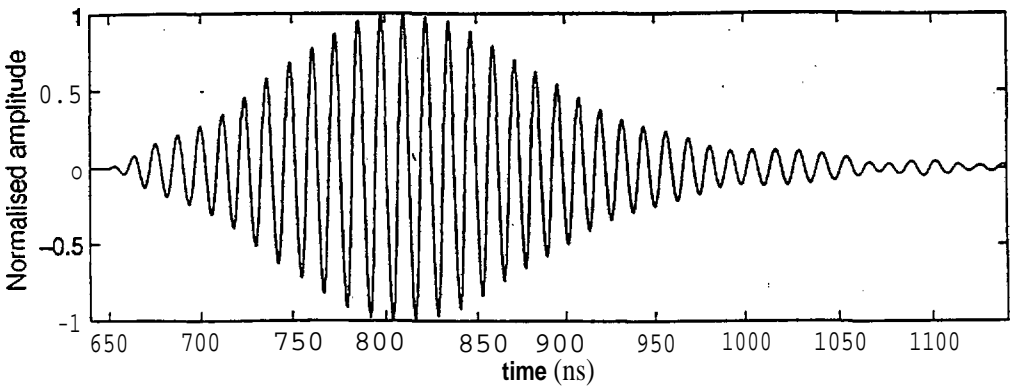


Fig 8 Typical 'CW' SAW signal

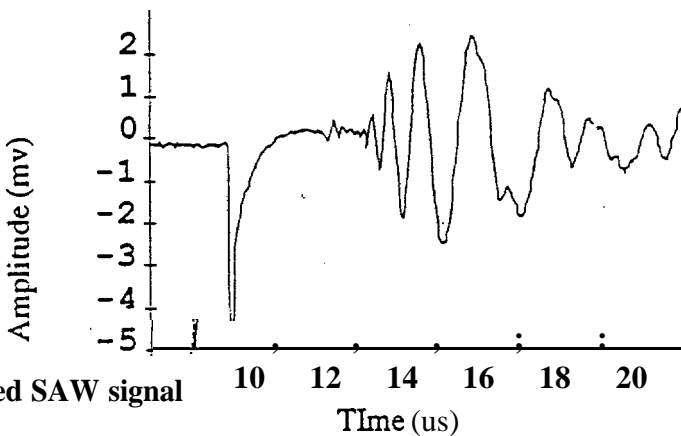


Fig 9 Typical pulsed SAW signal

6. Results

6.1. Measure SAW velocity in ideal samples at different states of stress

The main task of the CW system was to demonstrate the effect of stress on V_{SAW} and **measurements were performed on silicon nitride and steel samples with different states of stress using the stressing jigs. The results are shown in Fig 10. for SiN . The measurement on a steel sample (A2M2) is shown in Fig 11.**

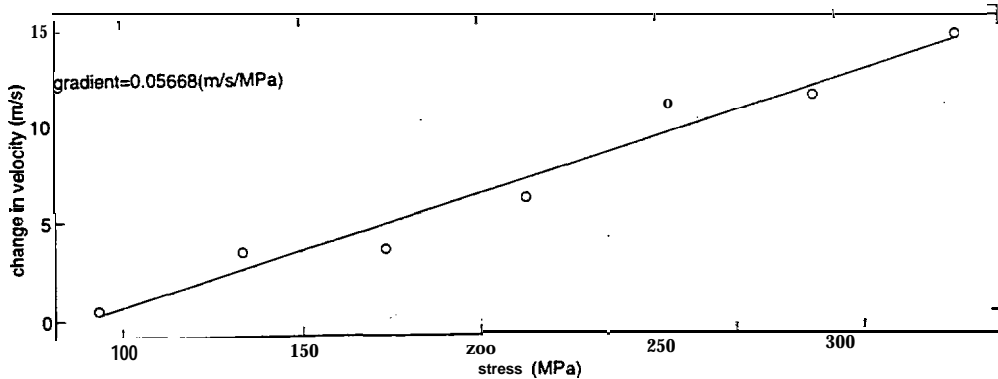


Fig 10 Experimental curve of SAW velocity on ceramic sample SS94 v applied tensile stress

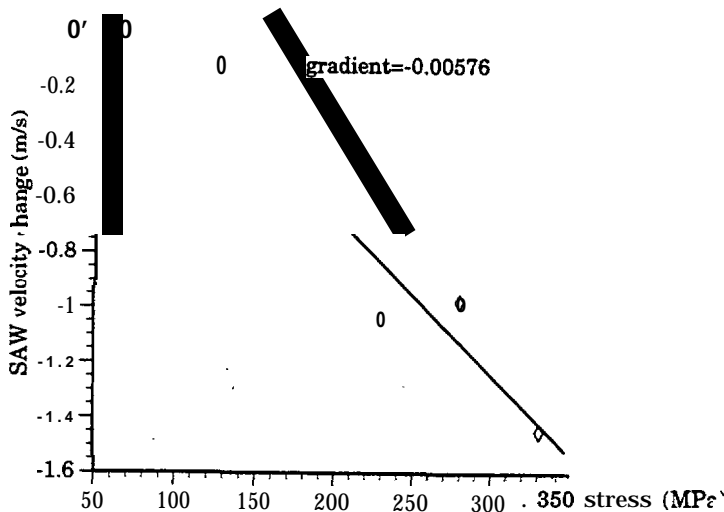


Fig 11 Experimental curve of SAW velocity on steel sample v applied tensile stress

6.2 Evaluation of pulsed laser system

The steel and ceramic materials specified and fabricated by the partners were examined and SAW velocities were measured using the hardware and software developed. The waveforms recorded on the **aluminium** sample show the SAW at a delay of $5\mu s$ from the generating pulse. The separation between **pulse** and probe beams was 2.5cm giving a value for the SAW velocity of $\approx 5000 \text{ ms}^{-1}$. (Compares with a textbook value of 4920 m^{-1}). This experiment **was** repeated at a range of incident **pulsed** laser powers **from** 10 to 50 **mJ**. This range **included** both the ablation and sub-ablation regimes **as** shown in Figs 12a,b & c where the change in acoustic wave shape is characteristic of the transition between the two regimes.

Experiments with **alumina** and silicon nitride using the integrated system have demonstrated the laser generation and detection of acoustic waves on ceramic materials. Signal processing algorithms were developed for improving the S/N ratio of the captured SAW trace. In particular, subtraction of the baseline trace which shows electrical and optical **interference** due to the pulsing laser from the recorded **signal** which exhibits the same masking noise enabled a dramatic improvement in signal.

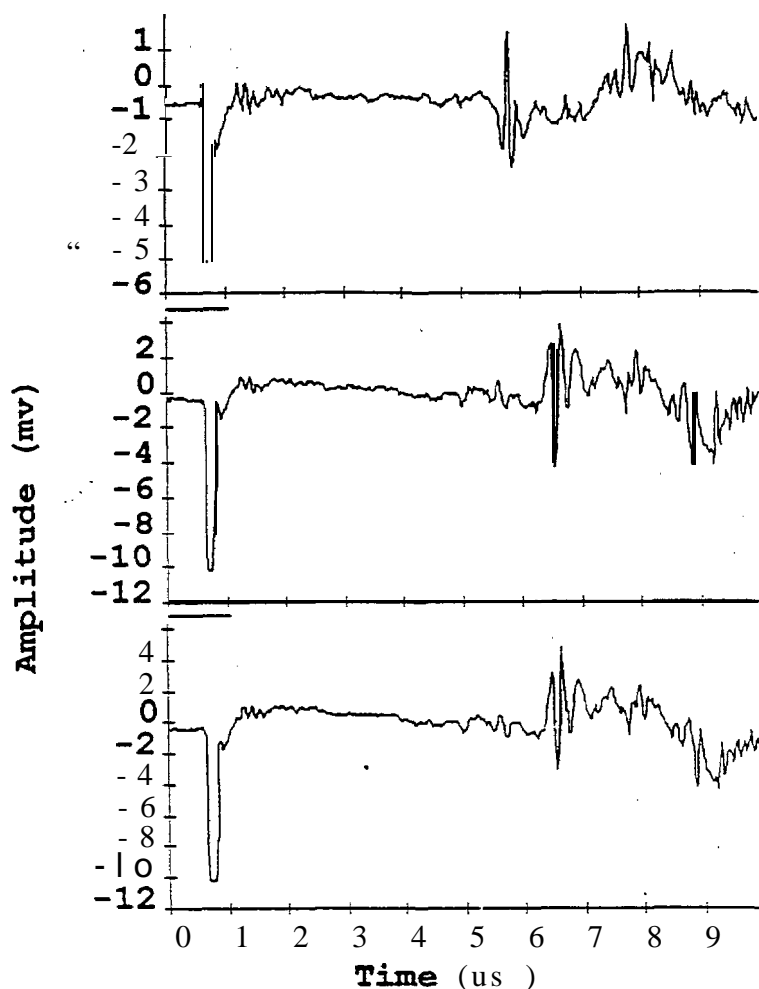


Fig 14 a, b& c Plots of acoustic waveform on aluminium at different incident laser energies. The onset of ablation is marked by a change in pulse shape, where the pulse goes leading edge negative to positive

6.3. Pulsed V_{SAW} on ideal samples

Low temperature co-fired ceramics are increasingly used in microelectronic packaging applications because of their, thermal expansion match to silicon, their excellent **dielectric** properties **and**, in line with other ceramics, their structural and high temperature properties. SAW waves were generated and detected on samples of **boro-silicate** glass doped with **aluminium** and **calcium** and LTCC with Zinc, Barium and Cobalt additives. A comparison of **the** traces shows that the velocities show significant variations (3187 ms^{-1} for the Al/Ca doped sample, 3100 ms^{-1} for the Zn/Ba/Co doped sample). These differences can form the basis of a rapid inspection system, The velocity of SAWS generated on a set of silicon nitride samples has also been measured as part of the mechanical testing exercise.

6.4. Bench marking of C-MAW instruments

In benchmarking the instrument, a detailed comparison of the SAW velocity measurements made using the C-MAW pulsed and CW probes has been undertaken to ensure that both instruments are giving reliable data. Measurements have also been made on a series of samples which have been analysed as part of the sample validation. Table 2 details the V_{SAW} measurements made on project samples and a comparison of velocities measured by both C-MAW systems and the accurate Vz methods used at Oxford University. These results show that the newly developed non-contacting method gives similar values to the best practice Vz technique, without the need for extreme controls.

Table 2 Table of SAW velocities recorded by NMRC, U of Nott and U of Oxford

Sample code	NMRC	Nottingham	U Oxford (Vz)
SS20	5537	5524.2	5522.7
SS30	5522	5543.1	5543.9
SS40	5784	5797.1	5783.9
SS50	5767	5773.5	5763.0

One of the large stress calibration silicon nitride sample (SS82) was exposed to the ND:YAG high power laser at full, 1/2 and 1/4 power settings. The laser track at full power was clearly visible, but the other two tracks did not show up under ultraviolet illumination after processing with fluorescent penetrant. It can therefore be concluded this is a truly nondestructive technique when operated at low power levels which still give accurate measurements.

6.7. Linking V_{SAW} to mechanical properties

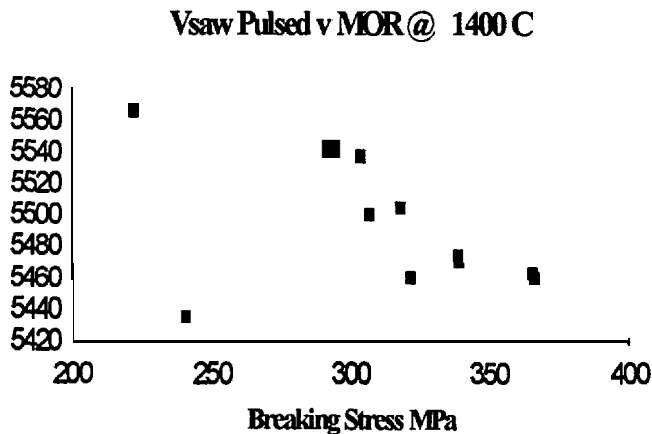


Fig13 V_{SAW} v MOR for bars manufactured at 1400 °C

6.9. Conclusion to MOR tests

The results in Fig 14. show a trend in the expected direction but the size of the change in V_{SAW} is much greater than the stress calibration work would suggest, The material is known to have a low Weibull modulus to its mechanical test results and a variable consistency. The V_{SAW} results probably indicate a greater sensitivity to this variation than previously seen in the more consistent material used for the stress calibration tasks.

7. Conclusions

The following conclusions have been made:-

1. The change in V_{SAW} with stress is measurable and repeatable. A change of **12m/s** is seen in silicon nitride bars when a stress of 300MPa is applied. The **nominal** velocity is **5586m/s**
2. **High**, single frequency (**82MHz**) SAW generation was demonstrated to be a **practical** method, using a tone burst system. Tone burst generation is preferred to **full** CW as reflections from edges and ends **can** be avoided using time **gating**.
3. **CW** generation is possible using the moving grating **method**, and different frequencies can be achieved. The amplitude of the SAW generated is too low for **non-contact** detection
4. V_{SAW} and best practice V_z measurement accuracy's were demonstrated as comparable using both the **CW** and pulsed V_{SAW} systems.
5. The pulsed C-MAW system **can** accurately measure the velocity and attenuation of SAWS propagation over short (**2mm**) and long (**40mm**) distances on ceramic substrates and is being used to characterise these materials.
- 6 The CW C-MAW system **can** accurately measure velocity and attenuation of SAWS over short (**<1mm**) and long (**>50mm** on spheres and cylinders) distances on samples with good surface finishes (O. **1 μ m**)

8. Acknowledgements

The **project** would like to thank the following for supporting the work and contributing to the development of this new technique.

The European Community for supporting the project (C-MAW, Contract No. **BREU** CT91 0563, Project No. **BE** 4398).

Newcastle University, UK, for phase analysis on ceramic samples.

Glasgow University, **UK**, for manufacturing tailored zone plates used to focus the SAW in the CW system.

Karlsruhe University, Germany, for the loan of a line focus acoustic microscope transducer.

Oxford University, UK, for making comparative measurements using their V_z system.

University of **Bayreuth**, Germany, for plasma etching of silicon nitride.